Digest Journal of Nanomaterials and Biostructures Vol. 7, No. 3, July - September 2012, p. 1179 - 1187

THE COMPLEX IMPEDANCE BEHAVIOR OF ZnO PARTICLES SYNTHESIZED VIA FAST CRYSTALLIZATION PRECIPITATION TECHNIQUES

M. D JOHAN OOI, A. ABDUL AZIZ*, M. J ABDULLAH, N. H. AL-HARDAN
School of Physics, Universiti Sains Malaysia, 11800 Penang, Malaysia

ZnO particles were synthesized via fast crystallization of precipitation technique by dissolving zinc and iodine in ethanol. The synthesized ZnO particles are pure and exhibits hexagonal wurtzite structure with the preferred orientation growth in (101) plane. The crystallite size is about 50 nm whereas FE-SEM images shows nearly spherical shape with the grain size of approximately 0.6 μm. The shape and size of the particles have a great influence on the impedance spectroscopy; therefore it is directly related to the conductivity of ZnO particles. The complex impedance of the MSM ZnO thick film shows two distinguished semicircles in which these arcs show a decrease in its diameter as the bias voltage increases from 0 to 5 V. The modeling of the MSM reveals that the bias voltage affects mainly the grain boundary components with the grain boundary resistance decreasing from approximately 207 MΩ to 40 MΩ, while the grain boundary capacitance increases from 5.14 pF to 43 pF as the bias voltage increases from 0 to 5 V.

(Received April 6, 2012; Accepted August 13, 2012)

Keywords: Chemical synthesis, Crystal growth, Impedance spectroscopy

1. Introduction

Zinc oxide (ZnO) with its direct wide band gap ~ 3.37 eV at room temperature makes it a good candidate for different advance application such as the transparent conducting oxide layer (TCO) in solar cell and display panels [1]. Furthermore, its large exciton binding energy (60 meV) makes it a good substituting material for replacing gallium nitrite (GaN) in optoelectronic application especially in the UV region [2, 3]. Advanced applications such as UV light emitting diodes (LED) and laser diodes (LD) have been reported for ZnO at room temperatures as well as in high temperatures [4]. Moreover, ZnO usage in sensing applications was also widely reported; sensors for gases [2], surface acoustic wave (SAW) [3] and photodetector at visible to UV wavelength region [5-7] whereas for ZnO nanostructures, there are a wide variety of applications as ZnO nanocantilevers, nanosensors, nanoactuators and nanolasers devices [8].

One of the main reasons why ZnO thin films are continuously being developed is that it can be prepared by using different techniques such as chemical vapor phase deposition (CVD), pulse laser deposition (PLD), sputtering and molecular beam epitaxy (MBE) [1,8]. Instead of the successful depositing thin film using these physical methods, high cost of maintenance is usually required for maintaining the equipment and the production is only limited to small scale. Meanwhile, wet chemical synthesis such as sol-gel [9], hydrothermal [10], colloid [11], sonochemical [12] and precipitation [13] often yields large-scale production, does not need expensive raw material and only requires low cost equipment. Moreover, these preparative techniques allow us to synthesize and control a uniformly structure and size of the particles down to nanometer scale. Therefore, there are many intensive researches efforts which focused on synthesizing ZnO via chemical method.As for realization of device, we need to study the electrical properties of the materials.

*Corresponding author : lan@usm.my

However, there are relatively few works which studied on the electrical characterization of ZnO particles in thin films via chemical method whereby most of the works are focused on the sol gel techniques [9, 15-17]. Despite of low cost, sol-gel technique often is time consuming where careful ageing and drying are required [18]. In contrast to sol gel, precipitation method is fast, large-scale production, require inexpensive precursor and only involves simple reaction. Precipitation in theory generally involves the simultaneous and rapid occurrence of nucleation and growth as well as the presence of secondary process such as agglomeration. It requires high super-saturation at which the nucleation takes places ensures that primary nucleation rates are high, thus produces a large number of grains [19]. The microstructure of these grains will affect the conductivity of ZnO whereby a small point defect and impurities can significantly affect the electrical, magnetic, and optical properties of the material.

Impedance spectroscopy (IS) is considered to be a powerful tool of analyzing the electrical properties of polycrystalline material. By changing the applied frequency of the system, different contributions of the electrodes, grain boundaries and individual grains can be distinguished [20, 21], whereby, the conductivity of material can be determined via charge transport of the grain and through the grain surface as well as via barriers formed on crystallite boundaries. Thus, by investigating the impedance spectroscopy, we can study the charge transport mechanism that contributes to the conductivities of material.

The complex impedance as a function of angular frequency (□) can be written as [20];

$$Z^*(\omega) = Z'(\omega) - iZ''(\omega) \quad (1)$$

Where, the Z' (ω) and Z''(ω) are the real and imaginary part of the complex impedance. For a device with a polycrystalline material the total impedance Z_T can be written as [21];

$$Z_T = Zg + Zgb + Zc \quad (2)$$

Where, Zg , Zgb, and Zc represent the complex impedance contribution of the grains, grain boundaries, and the electrode contacts, respectively. Each can be represented in the form of a parallel resistance (R) and capacitance (C).

In this work, ZnO was prepared using the fast crystallization of precipitation techniques and the electrical characteristic of ZnO particles was studied in order to understand the charge transport mechanism using the impedance spectroscopy.

2. Experimental details

Our work is generalized from the work of Wang et.al [22] with some extension and modification made in order to improve the uniformity and formation of ZnO particles. The ZnO particles were synthesized using high purity reagent raw materials. Zinc (Zn) and iodine (I_2) powder were supplied from Sigma-Aldrich whereas; absolute ethanol (C_2H_5OH) was obtained from Systerm Ltd. and diethanolamine ($NH(CH_2CH_2OH)_2$) from R & M Chemicals. All chemicals were used as received without further purification. In this synthesis, 0.5 g iodine powder was dissolved in 20 ml of absolute ethanol under constant magnetic stirring at room temperature. Then, 0.3 g zinc powder was added into the solution in parallel to oxygen diffusion at 0.6 sccm during the reaction. The solution gradually turns from dark red to grey within 1 hour indicating that the solution has fully reacted. After one hour of reaction, 0.5 ml diethanolamine was added drop wise while constantly stirring. White sediment was observed on the third hour of vigorous stirring. The sediment was then filtered and washed thoroughly with absolute ethanol followed by de-ionized water for several times to removes impurities. Finally, the precipitate was heated at 1150 °C for 3 minutes to dissociate ZnO_2^{2-} into ZnO particles and to remove the by-products of ZnO. White powdery product was obtained after this heat treatment. The structural properties of ZnO particles in the powdery forms was analyzed using X-ray powder diffractometer (XRD) using Siemens

XRD D5000 at a scanning rate of 0.05° per step with 2θ ranging from 10° to 80° at room temperature using CuKα radiation (λ = 0.15418 nm). The morphology of the sample was characterized using the Scanning Electron Microscope (SEM), Model JSM-6460 LV and Hitachi S4500 field emission scanning electron microscope (FE-SEM).

To study the complex impedance of prepared ZnO, an MSM (metal-semiconductor-metal) structure was fabricated. First, the agglomerated powder was crushed by an Agate mortar to form a fine grain powder. A paste was prepared by mixing the synthesis ZnO powder with organic binder Polyvinyl alcohol (PVA) and Isopropanol, and then screen printed it on an Al_2O_3 substrate (10 mm x 10 mm) coated by parallel Platinum (Pt) electrodes with the distance 0.70 mm apart. The obtained thick film was dried in an oven at 100°C for 10 minutes. It was then moved to a controllable tube furnace for further thermal treatment at 500° C for 30 minutes in an ambient atmospherically conditions.

The prepared thick film of Pt/ZnO/Pt MSM was measured by the Agilent impedance analyzer model 4294A at the frequency range from 40 Hz to 2 MHz with voltage amplitude of 500 mV. The unit was first calibrated to eliminate the effect of the leads. The impedance analyzer unit was controlled by a PC using LABVIEW 8.5 software via a GPIB interface. The effect of the bias voltage from 0 to 5 V will be studied. The measurements were performed at ambient conditions (the temperature was around 25°C and the humidity was around 62%).

3. Results and discussion

3.1 Structure of the films

Fig. 1 shows the X-ray diffraction pattern of the as-prepared ZnO sample. The peaks can be indexed on the basis of hexagonal wurtzite structure of the ZnO based on JCPDS card No. 01-070-8070. The calculated cell parameters of the prepared ZnO was a = 0.3246 nm and c = 0.5211 nm which are near to the identical standard values of bulk ZnO (a = 0.3249 nm and c = 0.5205 nm). No characteristic peaks were observed for other impurities, which revealed that the ZnO prepared was pure. The diffraction intensity and the line broadening are related to the crystallinity and crystallite size. The crystallite size D can be calculated according to Scherrer equation [23].

$$D = \frac{0.9\lambda}{\beta \cos\theta} \tag{3}$$

Where, λ is the wavelength of the X-ray radiation, β is the line broadening at half of the maximum intensity (FWHM) in radians and θ is the Bragg angle, respectively. By using the line broadening (FWHM) of the (101) ZnO phase, the crystallite size was approximately 50 nm.

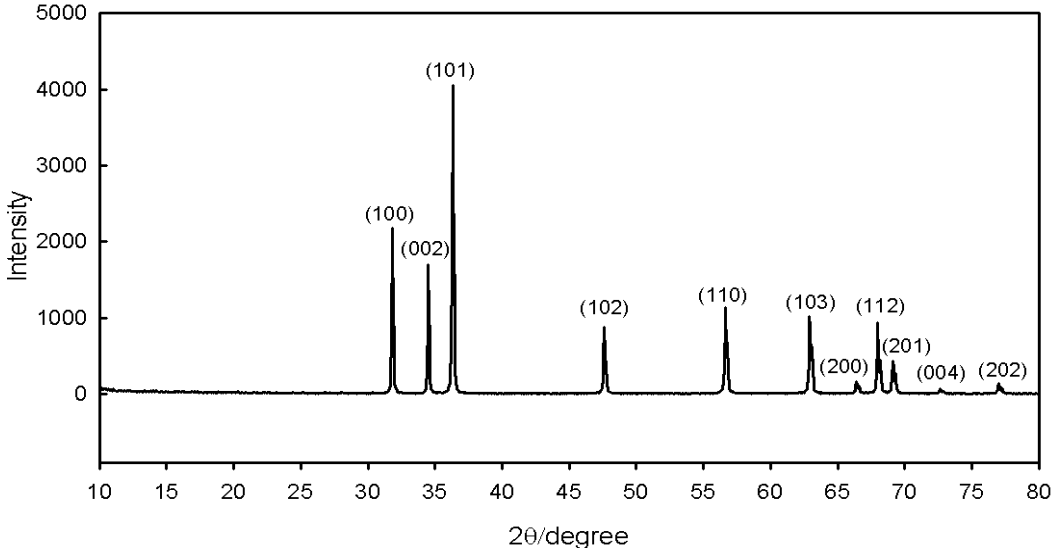

Fig. 1. X-ray diffraction pattern of ZnO particles powder after 3 hours of reaction.

The texture coefficient (TC) represents the texture of a particular plane, in which the deviation from unity implies preferred growth. The coefficient may be determined using the following formula [23];

$$TC\ (hkl\ ) = \frac{I\ (hkl\ ) / I_o\ (hkl\ )}{(1/n)\sum_n I\ (hkl\ ) / I_o\ (hkl\ )} \tag{4}$$

Where, *I(hkl)* is the measured XRD relative intensity of a plane *(hkl), I_o(hkl)* is the standard intensity of the plane *(hkl)* taken from JCPDS (01-070-8070) data card and N is the number of diffraction peaks considered. A sample with *TC (hkl)* =1 is said to exhibit randomly oriented crystallites while values larger than 1 indicate the abundance of crystallites oriented in the (*hkl*) direction. The TC *(hkl)* values were calculated for the strongest peaks of (100), (002) and (101) planes and are presented in Table 1. It can be seen that the highest *TC (hkl)* was in (101) plane. Thus, it became the preferred plane for the orientation growth.

Table 1: The values of texture coefficient (TC) and intensity of (100), (002) and (101) plane

Plane (*hkl*)	Standard XRD data From JCPDS 01-070-8070		Experiment		TC (*hkl*)
	2θ	Intensity (I_o)	2θ	Intensity (I)	
100	31.778	433	31.826	2185	0.592
002	34.434	194	34.469	1706	1.031
101	36.265	345	36.338	4054	1.378

Figure 2 shows the scanning electron micrographs of ZnO particles in powdery forms after 3h of reaction. From the micrographs, we can observe the formation of porous cluster of particles. The ZnO particles appear nearly spherical despite of some agglomeration occurs at the inter-particle separation.

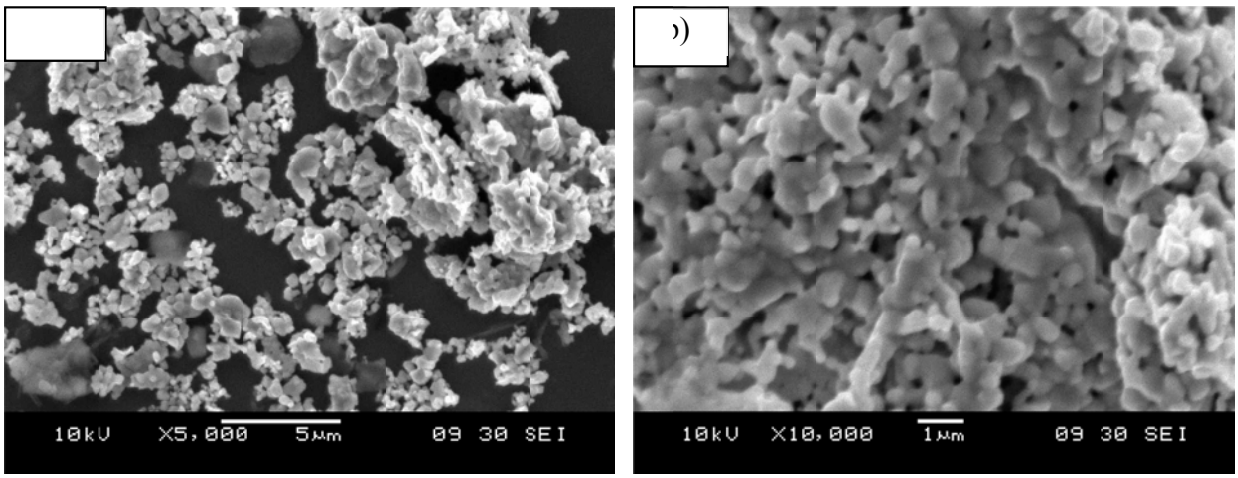

This agglomeration arises due to small particles which tend to aggregate in order to reduce its free energy and attain chemical stability. Meanwhile, the formation of porous cluster of ZnO is probably due to random attachment that results from aggregation which depends on the surface chemistry of the particles [25].

The mechanism of the reaction is proposed as below:

$$2C_2H_5OH + I_2 \rightleftharpoons 2(CH_3CH_2IOH) \quad (5)$$

$$2(CH_3CH_2IOH) + Zn^{2+} \longrightarrow Zn(OH)_2 + 2(CH_3CH_2I) \quad (6)$$

$$Zn(OH)_2 + 2OH^- \longrightarrow ZnO_2^{2-} + H_2O \quad (7)$$

$$ZnO_2^{2-} \longrightarrow ZnO \quad (8)$$

The reaction during the process of dissolving iodine in ethanol can be explained by equation (5) which is based on the charge transfer complexes mechanism. The unshared pair of electron in ethanol molecules will be donated to iodine molecules, which act as an electron acceptor. Meanwhile, Zn^{2+} ion will complex strongly with lone pair electron of O_2 and weaken the C-O bond to form $Zn(OH)_2$ and produces ethyl iodide as the byproducts. The diffusion of O_2 during the reaction will enhance the reaction rate by acting as a catalyst.

Equation (7) explained the reaction during the addition of diethanolamine ($NH(CH_2CH_2OH)_2$) after the reaction has fully reacted where diethanolamine forms OH^- , act as precipitator and forming a thick layer of organic molecules known as steric barrier on the surface [10] thereby acting as a capping agent.

Compared to other anion such as acetate, halide anions absorb more strongly on the surface and shows lower ion diffusion rate [24]. Thus, iodine is believed to have more control on the formation and nucleation of the particles. Zn metal powder which is superfluous comparing to iodine ensures the completion of $Zn(OH)_2$ and the occurrence of high super-saturation in the solution. This high super-saturation will yield ZnO_2^{2-} precipitate at which the nucleation process will take place whereby a large number of ZnO_2^{2-} nuclei or particles will be produced until the super-saturation is depleted. The formation of ZnO occurs due to heterogeneous nucleation and growth from initially formed ZnO_2^{2-} precipitate and finally dissociate into ZnO by thermal decomposition.

Fig. 3 shows the FE-SEM images of the prepared ZnO as a thick film after calcinations. The image reveals a uniform size of the ZnO grains with average size of 0.6 □m as measured by the FE-SEM. The reason for the increase in size compared to XRD result is because of the grain itself consists of many crystallites forming a cluster of particles. Thus, the FE-SEM images show the cluster of crystallite whereby the size of these crystallites is approximately 50 nm.

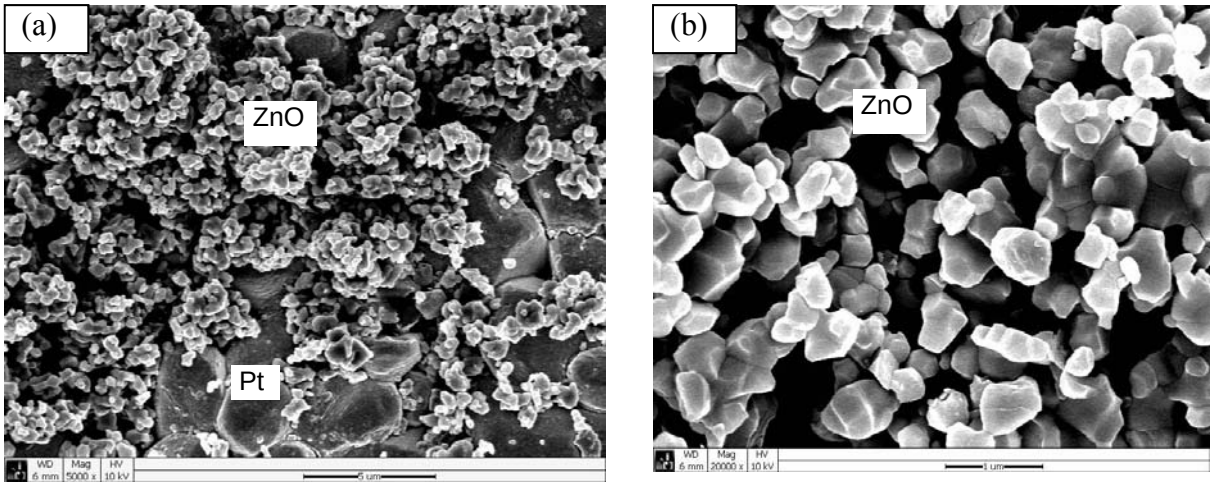

Fig. 3. FE-SEM micrographs of the thick film of the prepared ZnO particles after thermal treatment at 500^{o} C for 30 min. (a) at magnification x 5k, (b) at magnification x20k.

The impedance behavior of the MSM ZnO is shown in Figure 4. The figure shows the relation between the real and imaginary parts of the complex impedance. Evidently, the MSM device has two arcs. However, both arcs shrunk as the bias voltage increased from 0 to 5 V. Initially, the device components exhibit different relaxation times as the impedance behavior shows two arcs [20]. The relaxation time between the different components changes and the difference between them is clearly noticeable as both arcs of the impedance behavior become significant as the bias voltage increases.

The modeling of the impedance semicircles using the Zview software (from Scribner Associates Inc.) revealed that it contained a pair of parallel resistance and capacitance connected in a series. The initial data of both R and C were estimated manually at each bias voltage, where R is estimated from the diameter of the arc (R= 2Z') in Fig. 4, and C is given by the relation $\omega_{max}RC = 1$.

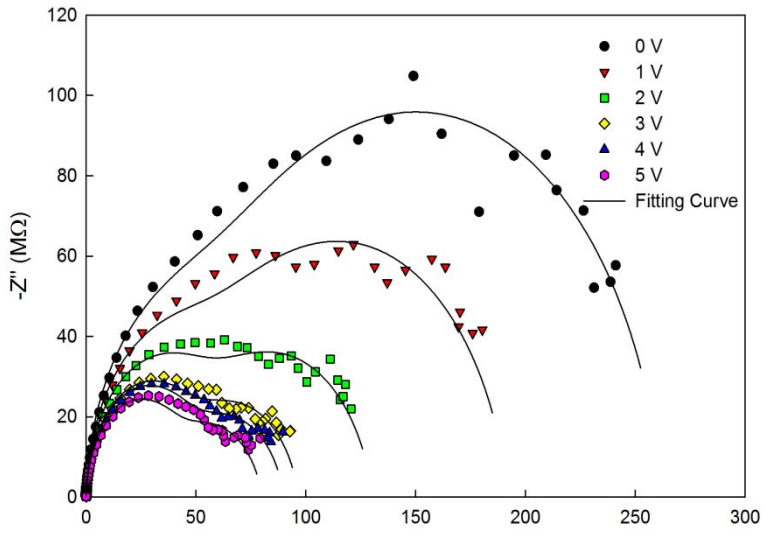

The proposed model of the ZnO MSM can be represented by a parallel equivalent circuit of RC connected in a series with a single resistance, as shown in Figure 5.

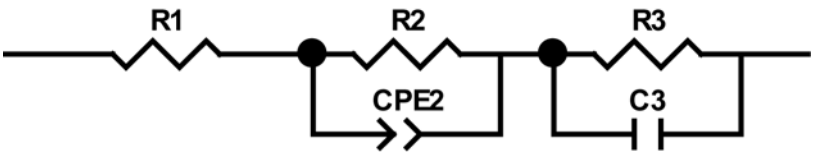

Fig. 5: The proposed model of the thick film ZnO

The estimated values of the components of the proposed equivalent circuit are tabulated in Table 2.

Table 2: Rs and Cs values representing the fitting data of ZnO MSM

Bias Voltage (V)	R1 (Ω)	R2 (MΩ)	C2 (CPE) (pF)	p	R3(MΩ)	C3 (pF)
0	1340	206.96	5.14	0.91	54.96	1.02
1	1250	139.41	8.51	0.89	52.81	0.92
2	1340	77.52	18.46	0.86	52.75	0.79
3	1360	50.12	29.52	0.85	46.61	0.74
4	1480	43.69	40.20	0.83	46.41	0.72
5	1600	39.99	42.75	0.82	40.18	0.74

Clearly, based on the tabulated data, R1 and R3 do not change significantly, whereas R2 is affected by the bias voltage. The capacitance connected to R3 shows the same behavior, whereas the capacitance connected to R2 is affected by the bias voltage. As R1, R3, and C3 show no significant change as the bias voltage changes, these components may represent the grain resistance (R1), contacts' resistance (R3), and the contacts' capacitance (C3), whereas R2 and C2 (CPE) represent the grain boundary of the ZnO.

The value of the C2 best fits the constant phase element (CPE), which is often used to describe the behavior of polycrystalline materials with a distribution in their electrical properties

due to the material inhomogeneity (e.g., in the grain boundary) that gives rise to a distribution of the respective relaxation times. The impedance of a CPE is given by [26, 27]

$$Z_{CPE} = \frac{1}{A(\iota\omega)^p} \tag{8}$$

where, A is a constant, and p is a dimensionless parameter with the value of less than unity. As p = 1, then the equation represents a characteristic of a capacitor with A = C.

The behavior of the MSM ZnO under different bias voltages can be explained by the bias voltage affecting mainly the barrier height between the grains (the grain boundary region). Consequently, this reduces the height and carries more to cross the barrier, which results in decreasing the resistance of the grain boundary region. In contrast, the capacitance of the grain boundary region increases with the increasing bias voltage. This is due to the accumulation of the charge at the grain boundaries.

4. Conclusion

In summary, ZnO particles were prepared by using the fast crystallization of precipitation technique. The XRD spectra indicate that the synthesized ZnO particles are of a polycrystalline structure with preferred orientation growth in (101) plane. The grain size is about 0.6 μm whereas the crystallite size is approximately 50 nm. The complex impedance of the ZnO prepared as a thick film showed two semicircles. The arcs of the semicircles show dependence on the applied bias voltage. The bias voltage affects mainly the conductivity through the grain boundary components (R2 and C2 (CPE)).

Acknowledgement

This work has been supported by the Universiti Sains Malaysia through a short-term Grant USM RU-PRGS.

References

[1] K. Ellmer, A. Klein, B. Rech (Eds), Transparent Conductive Zinc Oxide Basics and Applications in Thin Film Solar Cells, Springer-Verlag Berlin Heidelberg 2008.
[2] C. Jagadish and S.J. Pearton (Eds), Zinc Oxide Bulk, Thin Films and Nanostructures: Processing, Properties and Applications, Elsevier, Oxford.
[3] H. Morkoç and Ü. Özgür, "Zinc Oxide : Fundamentals, Materials and Device Technology:, 2009 WILEY-VCH Verlag GmbH & Co.
[4] M. Willander, O. Nur, Q. X. Zhao, L. L. Yang, M. Lorenz, B. Q. Cao, J. Zuniga Perez, C. Czekalla, G. Zimmermann, M. Grundmann, A. Bakin, A. Behrends, M. Al-Suleiman, A. El-Shaer, A. Che Mofor, B. Postels, A. Waag, N. Boukos, A. Travlos, H. S. Kwack, J. Guinard and D. Le Si Dang, Nanotechnology **20,** 332001 (2009).
[5] T. Zhai, X. Fang, M. Liao, X. Xu, H. Zeng B. Yoshioand D. Golberg, Sensors **9**, 6504 (2009).
[6] C. Soci, A. Zhang, B. Xiang, S. A. Dayeh, D. P. R. Aplin, J. Park, X. Y. Bao, Y. H. Lo, D. Wang, Nano Lett. **7**, 1003 (2007).
[7] J. D. Prades, R. J. Diaz, F. H. Ramirez, L. F. Romero, T. Andreu, A. Cirera, A. R. Rodriguez, A. Cornet, J. R. Morante, S. Barth, and S. Mathur, J. Phys. Chem. C **112**, 14639 (2008).
[8] T.K. Lina, S.J. Changa, Y.K. Sua, B.R. Huangb, M. Fujitac, Y. Horikoshi, J. Cryst. Growth **281**, 513 (2005).
[9] M. Ristic, S. Music, M. Ivanda, S. Popovic, Journal of Alloys and Compounds, **397**, L1 (2005).

[10] Yu Chen, Runzhou Yu, Qian Shi, Jingli Qin, and Feng Zheng, Materials Letters, **61,** 4438 (2007).
[11] L. Dong, Y.C. Liu, Y.H. Tong, Z.Y. Xiao, J.Y. Zhang, Y.M. Lu, D.Z. Shen and X.W. Fan, Journal of Colloid and Interface Science, **283**, 380 (2005).
[12] Raghvendra S. Yadav, Priya Mishra and Avinash C. Pandey, Ultrasonics Sonochemistry **15**, 863 (2008).
[13] S.C. Zhang and X.G. Li, Colloids and Surfaces A: Physicochem. Eng.Aspects **226**, 35 (2003).
[14] R. Nagarajan, "Nanoparticles: Building Blocks for Nanotechnology", ACS Symposium Series, **996,** 2 (2008).
[15] E A. Meulenkamp, J. Phys. Chem. B **102**, 5566 (1998).
[16] Naoko Asakuma, Hiroshi Hirashima, Hiroaki Imai, Toshimi Fukui and Motoyuki Toki, Journal of Sol-Gel Science and Technology, **26**, 181 (2003).
[17] Junying Zhang, Haibing Feng, Weichang Hao and Tianmin Wang, Journal of Sol-Gel Science and Technology **39**, 37 (2006).
[18] Chung-Hsin Lu, Yuan-Cheng Lai and Rohidas B. Kale, Journal of Alloys and Compounds **477**, 523 (2009).
[19] D. Sun, M. Wong, L. Sun, Y.Li, N. Miyatake and H.J Sue, J. Sol-Gel Sci.Technol **43,** 237 (2007).
[20] J. R. Macdonald (editor) "Impedance Spectroscopy - Emphasizing Solid Materials and Systems", (John Wiley & Sons, New York, 1987).
[21] P. Knauth, J. Schoonman (Eds), "NANOCRYSTALLINE METALS AND OXIDES selected Properties and Applications", 2002 Kluwer Academic Publishers, p111.
[22] C.Wang, Q.Li, B.Mao, E.Wang and C. Tian Materials Letter **62**, 1339 (2008).
[23] Mario Birkholz Thin Film Analysis by X-Ray Scattering, 2006 WILEY-VCH Verlag GmbH & Co. KGaA, Weinheim.
[24] J. I. Pankove, Optical Processes in Semiconductors, 1971 Prentice-Hall Inc., Englewoord Cliffs, NJ.
[25] S. Sepulveda-Guzman, B. Reeja-Jayan, E. de la Rosa, A. Torres-Castro, V. Gonzalez-Gonzalez and M. Jose-Yacaman, Materials Chemistry and Physics **115**, 172 (2009).
[26] H. Baltes, W. Gopel and J Hesse (ed), Sensors update Vol. 1: Sensor technology – applications – markets, VCH, Weinheim, 1996. 2nd edition, p58.
[27] Seung-Hoon Choi, Guy Ankonina, Doo-Young Youn, Seong-Geun Oh, Jae-Min Hong, Avner Rothschild and Il-Doo Kim, "Hollow ZnO Nanofibers Fabricated Using Electrospun Polymer Templates and Their Electronic Transport Properties", ACS Nano **3,** 2623 (2009).